
Advection–Diffusion on Graphs: A Bakry–Émery Laplacian for Spectral Graph Neural Networks

Pierre-Gabriel Berlureau^{*1} Ali Hariri^{*2} Victor Kawasaki-Borruat^{*2} Mia Zosso^{*2} Pierre Vandergheynst²

Abstract

Graph Neural Networks (GNNs) often struggle to propagate information across long distances due to oversmoothing and oversquashing. Existing remedies such as graph transformers or rewiring typically incur high computational cost or require altering the graph structure. We introduce a Bakry–Émery graph Laplacian that integrates diffusion and advection through a learnable node-wise potential, inducing task-dependent propagation dynamics without modifying topology. This operator has a well-behaved spectral decomposition and acts as a drop-in replacement for standard Laplacians in spectral GNNs. Building on this insight, we develop μ -ChebNet, a spectral architecture that jointly learns the potential and Chebyshev filters, effectively bridging message-passing adaptivity and spectral efficiency. Our theoretical analysis shows how the potential modulates the spectrum, enabling control of key graph properties. Empirically, μ -ChebNet delivers consistent gains on synthetic long-range reasoning tasks, as well as real-world benchmarks, while offering an interpretable routing field that reveals how information flows through the graph. This establishes the Bakry–Émery Laplacian as a principled and efficient foundation for adaptive spectral graph learning.

1. Introduction

Graph Neural Networks (GNNs) (Scarselli et al., 2008; Bruna et al., 2013; Defferrard et al., 2016) have achieved significant success in recent years, driving the development of novel architectures and stimulating investigations into their theoretical foundations. Despite these advances, several limitations are now well documented, most notably repre-

sentational collapse, oversmoothing, and over-squashing (Shao et al., 2023; Rusch et al., 2023; Jin & Zhu, 2025; Attali et al., 2024). While their precise origins remain an active area of research (Arnaiz-Rodriguez & Errica, 2025), these phenomena are closely tied to information flow during backpropagation, motivating increased scrutiny of learning and inference dynamics in GNNs (Arroyo et al., 2025).

A fruitful line of work has sought to analyze and mitigate these limitations by interpreting GNNs through the lens of continuous dynamics (Poli et al., 2019). In particular, diffusion-based formulations recast message passing as the discretization of partial differential equations (PDEs) on graphs, enabling principled control over information propagation. Anisotropic diffusion models (Chamberlain et al., 2021a) were introduced with a learnable diffusivity to modulate and interpret node coupling strengths, while more recent advection-diffusion formulations (Wu et al., 2023a; 2025a) revealed similarities between learnable diffusivity and attention mechanisms, further implying the importance and efficiency of diffusion. Although the continuous GNN diffusion perspective provides a principled foundation for designing expressive architectures, it often leads to high computational complexity due to discretization.

Conversely, spectral GNNs (Defferrard et al., 2016; Kipf & Welling, 2017) offer simple and computationally efficient architectures by leveraging the Fourier domain of the graph, only requiring to learn the fixed spectral filters’ weights. Recent work (Gravina et al., 2023; Hariri et al., 2025) has shown that stabilized spectral architectures can outperform MPNNs and graph transformers on long-range tasks. However, classical spectral GNNs rely on a fixed graph Laplacian L , which limits their ability to adapt information flow to task-specific structure. In particular, they lack a mechanism for locally steering information propagation.

Contributions We present a principled extension of spectral GNNs, allowing more efficient information propagation without altering the graph topology. Building on ideas from Bakry–Émery theory (Bakry & Émery, 1985; Bakry et al., 2013), we show that such guided dynamics (advection) naturally arise from diffusion when considering an inner product space weighted by a node-wise potential μ , resulting in a

¹École Normale Supérieure – PSL, Paris, France ²École polytechnique fédérale de Lausanne (EPFL), Lausanne, Switzerland. Correspondence to: Victor Kawasaki-Borruat <vic-tor.borruat@epfl.ch>.

gradient flow driven by $\nabla\mu$. This observation leads to a novel class of graph Laplacians L_μ whose entries now depend on the potential μ (Figure 1). Once this structure is acknowledged, we propose to *learn the potential* μ , before feeding it downstream to a spectral GNN. Unlike generic edge-reweighting and attention schemes, this formulation introduces one degree of freedom *per node*. Our work makes the following contributions:

1. **A Bakry–Émery Laplacian for graphs.** We derive a discrete Bakry–Émery (BE) Laplacian whose entries depend on a learnable node-wise potential. This operator induces advection–diffusion dynamics on graphs without modifying the topology, providing a principled mechanism for steering information flow.
2. **Spectral analysis revealing controllable propagation dynamics.** We characterize how the potential reshapes the Laplacian spectrum, showing that it enables independent control of the spectral gap and spectral radius. This allows targeted mitigation of oversquashing and overmixing using a single scalar field, while preserving connectivity.
3. **A new family of spectral GNNs.** We introduce μ -ChebNet and μ -StableChebNet, architectures that jointly learn (i) a propagation dynamics via the potential μ and (ii) spectral filters via Chebyshev polynomials. These models combine the adaptivity of message-passing with the efficiency and global receptive field of spectral methods, requiring only minimal architectural changes.
4. **Extensive empirical evidence and interpretability.** Across synthetic long-range reasoning tasks and real-world benchmarks, our models outperform strong spectral GNNs and transformer-based approaches. The learned potentials provide interpretable routing fields, revealing task-dependent communication pathways that emerge naturally from training.

Outline Section 3 reviews background on graph Laplacians, advection–diffusion dynamics, and Chebyshev spectral filters. Section 4 introduces the Bakry–Émery Laplacian on graphs, analyzes its spectral properties, and shows how it enhances standard spectral GNNs, leading to our μ -ChebNet architecture whose results we show in Section 5. The latter benchmarks our model on synthetic and real-world tasks. We conclude by illustrating how the learned potential provides a simple and interpretable mechanism for task-dependent routing.

2. Related Work

MPNNs are a class of GNNs in which node representations are updated by aggregating messages from neighboring

nodes through learnable functions (Gilmer et al., 2017). This design offers flexibility but comes with limitations. In particular, their performance on long-range tasks is impacted, as the architecture intrinsically suffers from oversmoothing and oversquashing (Li et al., 2018; Alon & Yahav, 2021), which have been shown to be contractive effects during training (Arroyo et al., 2025).

Recent works propose diffusive PDE-based dynamics, with an emphasis on controlling the diffusivity to improve information flow. In GRAND (Chamberlain et al., 2021b) this control is achieved by a diffusivity matrix coupling various nodes of the graph, enabling non-local behaviour through attention-like mechanisms. In Wu et al. (2025b), they implement an analogous diffusivity, and cast advection as an adjacency-based message-passing mechanism that brings structural context back to the model. The presence of both driving and diffusive dynamics allows for a balance of graph-dependent (resp. independent) labels. While this approach is expressive and theoretically motivated, solving the full advection-diffusion equation is both computationally demanding and non-trivial. Moreover, the question of different advection choices remains open.

On the other hand, Graph Transformers (GTs) (Rampášek et al., 2022) offer a similar type of dynamics through local aggregation (advection) and global attention (diffusion). Sparser GTs (Shirzad et al., 2023; 2024; Chen et al., 2022) and dynamical graph-rewiring schemes (Arnaiz-Rodríguez et al., 2022) have also been proposed as alternative architecture, nonetheless incurring a strong computational cost.

Perhaps unexpectedly, spectral GNNs - such as ChebNets (Defferrard et al., 2016) - have shown a recent revival in relevance for both their computational efficiency and ability to capture global/long-range interactions via constructive graph Laplacian-based filters. While these models are simple to implement and analyze due to the rich tools of spectral graph theory (Chung, 1997), ChebNets have been shown to be prone to instabilities as their receptive field grows. Hariri et al. (2025) have recently overcome this issue by proposing Stable-ChebNet via anti-symmetric weights, enforcing volume-preservation of features (Gravina et al., 2023). Stable-ChebNet was also shown to consistently outperform MPNNs, graph rewiring techniques, and GTs on several long-range tasks, highlighting the continued relevance of spectral models. The generalization power of spectral GNNs to graph structure unseen at training is also largely still an open question. Experiments, including our own (Section 5), suggest that spectral GNNs transfer to unseen graphs and this is supported by theoretical findings (Wang et al., 2025; Levie et al., 2021).

3. Background

3.1. Graph Laplacians

Let $G = (V, E)$ be an undirected graph with $|V| = n$ vertices and $|E| = m$ edges. We associate to G its unnormalized graph Laplacian $L \in \mathbb{R}^{n \times n}$, defined as $L = D - A$ where $A \in \mathbb{R}^{n \times n}$ is the adjacency matrix of G and D is the diagonal degree matrix with entries $D_{ii} = d_i$.

$$[D]_{ii} = d_i = \sum_{j=1}^n [A]_{ij}. \quad (1)$$

The Laplacian is symmetric and positive semidefinite, and encodes the connectivity structure of the graph. As a consequence, L admits an eigenvalue decomposition of the form

$$L = U \Lambda U^\top, \quad (2)$$

where Λ is the diagonal matrix of eigenvalues $0 \leq \lambda_0 \leq \lambda_1 \leq \dots \leq \lambda_{n-1}$ and U is the orthogonal matrix of eigenvectors.

To define gradient and divergence operators on graphs, we denote by \mathcal{H}_V the Hilbert space of functions $f : V \rightarrow \mathbb{R}$ over the vertices, with corresponding scalar product $\langle f, g \rangle$. Likewise, \mathcal{H}_E will be the Hilbert space of functions $G : E \rightarrow \mathbb{R}$ defined over edges. We will typically use capital letters and write $G(i, j)$ or $G(e)$ to discriminate with vertex functions $g(i)$. The scalar product on \mathcal{H}_E is $\langle F, G \rangle = \sum_{(i,j) \in E} F(i, j) G(i, j)$. The graph gradient $\nabla^G : \mathcal{H}_V \rightarrow \mathcal{H}_E$ is given by

$$\nabla_{ij}^G f = f(j) - f(i) \quad (3)$$

for $(i, j) = e$ the edge between the nodes i and j . Note that an orientation has to be chosen for each edge. If the graph is undirected, we can choose it randomly as explained below. The divergence is defined as $\text{div } G = -2\nabla^{G^*}$ where the adjoint $\nabla^{G^*} : \mathcal{H}_E \rightarrow \mathcal{H}_V$ of the gradient is computed with respect to the inner products defined above. More precisely:

$$\begin{aligned} \langle \nabla^G f, G \rangle &= \sum_{(i,j) \in E} (f(j) - f(i)) G(i, j) \\ &= \frac{1}{2} \sum_i f(i) \sum_{j \sim i} (G(j, i) - G(i, j)) \\ &= \langle f, \nabla^{G^*} G \rangle \end{aligned}$$

which shows that $\nabla^{G^*} G(i) = \frac{1}{2} \sum_{j \sim i} (G(j, i) - G(i, j))$. With these definitions we have $L = -\nabla^{G^*} \nabla^G$ and that the Laplacian does not depend on the choice of edge orientations. Finally, the Dirichlet bilinear form associated to the graph is defined as $\mathcal{D}^G(f, g) = \frac{1}{2} f^\top L g, \forall f, g \in \mathcal{H}_V$.

3.2. ChebNet

With the quantities introduced above, we are now able to introduce ChebNets. The convolution operator on graph $*_G$ operates on the basis defined in equation (2) U like $x *_G y = U((U^\top x) \odot (U^\top y))$, with \odot the element-wise Hadamard product (Defferrard et al., 2016). For an undirected graph with Laplacian L , a graph signal $X \in \mathbb{R}^n$ can be filtered in the spectral domain as

$$Y = U g_\theta(\Lambda) U^\top X,$$

with g_θ a spectral filter. ChebNet approximates the latter using Chebyshev polynomials, which form an orthogonal basis on the space $L^2([-1, 1], \frac{dy}{\sqrt{1-y^2}})$: $g_\theta(\Lambda) \approx \sum_k^K \Theta_k T_k(\tilde{\Lambda})$, where $T_k(\tilde{\Lambda})$ is the k -th Chebyshev polynomial of $\tilde{\Lambda}$ with $\tilde{\Lambda} = \frac{2\Lambda}{\lambda_{\max}} - I, I$ the identity matrix, for the eigenvalues to lie in the domain of the polynomials. Therefore, the convolution operator defined above can be written as: $Y = \sum_k^K \Theta_k T_k(\tilde{L}) X$ where $\tilde{L} = \frac{2L}{\lambda_{\max}} - I$ and Θ_k is the Chebyshev coefficient. With this, the spectral convolution can be computed efficiently without the need of performing a spectral decomposition in $\mathcal{O}(Km)$ time (Defferrard et al., 2016).

Stable-ChebNet: As reported in (Hariri et al., 2025), while ChebNets are effective at modeling long-range dependencies, increasing the polynomial degree may introduce numerical instabilities. To address this issue, the authors propose controlling the spectrum of the Jacobian matrix by enforcing purely imaginary eigenvalues.

3.3. Advection–diffusion

To clarify our use of the terms *advection* and *diffusion*, as well as their relationship and distinction, we begin with the Euclidean setting. We start from the continuity equation:

$$\frac{\partial u}{\partial t} + \nabla \cdot \vec{j} = \alpha, \quad \vec{j} = \underbrace{-D(u, \vec{x}) \nabla u(\vec{x}, t)}_{\text{diffusion}} + \underbrace{\vec{v} u}_{\text{advection}}, \quad (4)$$

where $u(\vec{x}, t)$ is a scalar function of position $\vec{x} \in \mathbb{R}^d$ and time t , $\alpha(\vec{x}, t)$ is a source/sink term, $\vec{v}(\vec{x}, t)$ is a vector field and \vec{j} the flux of the quantity u , consisting of a diffusion term and an advection term. In the most general case, the diffusivity coefficient D is a two-rank tensor that specifies the magnitude and anisotropy of diffusion. It can depend on spatial coordinates and may also depend on $u(\vec{x}, t)$ itself. The diffusion equation is therefore generally non-linear, inhomogeneous and anisotropic. If D is a scalar function rather than a tensor, the diffusion is isotropic but may remain spatially inhomogeneous. In the simplest case, D is constant and diffusion is both homogeneous and isotropic. When $D = 0$ the equation describes the transport of the quantity u along the flow of the vector field $\vec{v}(\vec{x}, t)$. Assuming for

Ring graph, heat kernel at node 0 (highlighted)
without potential with potential

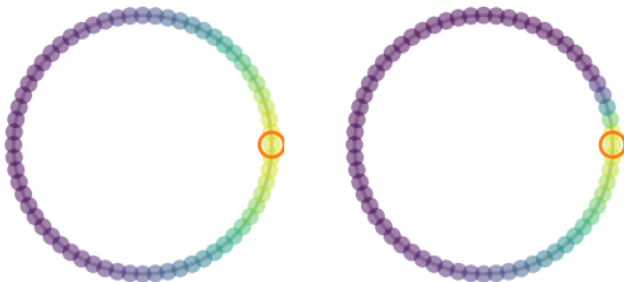


Figure 1. Standard vs. μ -Laplacian on a ring graph. (a) Heat diffusion under the standard Laplacian produces nearly isotropic propagation. (b) The μ -Laplacian induces an advection–diffusion geometry via a node-wise potential, biasing information flow without altering graph topology. The potential breaks the symmetry, resulting in anisotropic diffusion

simplicity that the field has zero divergence reduces (4) to:

$$\frac{\partial u}{\partial t} = \bar{v} \cdot \nabla u$$

whose solution for a smooth vector field is given by

$$u(\bar{x}, t) = \bar{u}(X(t, \cdot)^{-1} \bar{x}),$$

where $\bar{u}(\bar{x}) = u(\bar{x}, 0)$ and $X(t, \cdot) : \mathbb{R}^d \rightarrow \mathbb{R}^d$ is the flow map of the ordinary differential equation $\dot{\bar{x}}(t) = \bar{v}(\bar{x}, t)$. This shows that the solution at time $t + \epsilon$ is computed by fetching information at time t along the flow of the advection field.

While advection provides a principled way to steer information flow and mitigate oversquashing, existing graph-based formulations either require solving complex PDEs or introduce attention-like mechanisms that alter the graph structure. This motivates the search for a graph operator that incorporates advection directly into the Laplacian itself, preserving spectral efficiency while enabling task-dependent control of propagation.

4. Method

We consider solving (4) using a naive operator splitting scheme, alternating between a pure advection step and a pure diffusion step. For simplicity, we assume that the diffusion coefficient D is constant in (4). Over a single time step of size ϵ , the update can be interpreted as follows: for each $x \in \mathbb{R}^d$, we first consider all points $y \in \mathcal{B}(x, \epsilon)$ and evaluate the transported quantity $\bar{u}(X(\epsilon, \cdot)^{-1}(y))$. These values are then aggregated at x by applying the diffusion operator, i.e., by convolution with the heat kernel $e^{-\frac{1}{2}\epsilon\Delta}$.

This simplified scheme bears a striking resemblance to the basic primitives of Message Passing Neural Networks (MPNNs) (Gilmer et al., 2017; Battaglia et al., 2018). First messages are computed with dedicated message functions for all neighbors of a node and then these messages are aggregated and used to update the state of that node. We clearly see here that aggregation corresponds to the diffusion step, which is simply a weighted average, while messages are computed via the advection vector field, which provides local control over the flow of information.

Next, we note that the advection–diffusion equation (4) does not admit a straightforward extension to graph-structured domains. A natural approach is to replace differential operators with their graph counterparts, as done for example in Chamberlain et al. (2021b); however, this obscures several important issues. First, such discrete difference operators are not derivations: in general, they do not satisfy the Leibniz rule, and must therefore be handled with care. Second, graphs do not admit vector fields in the classical sense, and consequently the interpretation of the drift term in (4), or even of gradients as vectors, does not align well with our usual geometric intuition. In this section, we propose a mechanism to construct an advection-diffusion equation on graphs, respecting the underlying discrete adjacency and that does not suffer from the aforementioned limitations. We first formulate this construction in the continuous case for the clarity of the exposition and later adapt it to graphs in a transparent way.

4.1. The Bakry-Emery Laplacian on \mathbb{R}^d

In the continuous setting, we begin by introducing the key idea underlying our construction: *advection can arise naturally from diffusion when the underlying geometry is modified*. This avoids the need to explicitly define vector fields, which is rather crucial in the graph domain.

Let $f, g : \Omega \subset \mathbb{R}^d \rightarrow \mathbb{R}$ be smooth functions vanishing on the boundary $\partial\Omega$. We first recall the standard Dirichlet bilinear form

$$D(f, g) = \frac{1}{2} \int_{\Omega} (\nabla g \cdot \nabla f) dx, \quad (5)$$

which measures the smoothness of functions over the domain. There exists a unique symmetric, positive-definite operator L such that

$$\mathcal{D}(f, g) = \int_{\Omega} dx g L f = \int_{\Omega} dx f L g.$$

To introduce directional bias into the dynamics without modifying the operator itself, we *change the geometry of the space* by weighting the underlying measure. Specifically, we consider a non-negative density $\mu(x) = Z^{-1}e^{-V(x)}$, which induces a weighted inner product and reflects spatial preference encoded by the potential V . Using this density,

we define the weighted Dirichlet form

$$\mathcal{D}_\mu(f, g) = \frac{1}{2} \int_\Omega dx \mu(x) (\nabla g \cdot \nabla f). \quad (6)$$

Proposition 4.1 (Bakry–Émery operator as weighted diffusion). *Let $\Omega \subset \mathbb{R}^d$ be a smooth domain and let $\mu(x) = Z^{-1}e^{-V(x)}$ be a strictly positive, integrable density on Ω , with $V \in C^1(\Omega)$. Define the weighted Dirichlet form*

$$\mathcal{D}_\mu(f, g) = \frac{1}{2} \int_\Omega \mu(x) \nabla f(x) \cdot \nabla g(x) dx, \quad f, g \in C_0^\infty(\Omega).$$

Then \mathcal{D}_μ admits the generator L_μ given by

$$L_\mu f = -\frac{1}{2}(\nabla \log \mu \cdot \nabla f + \Delta f) = \frac{1}{2} \nabla V \cdot \nabla f - \frac{1}{2} \Delta f \quad (7)$$

We therefore recover the Bakry–Emery Laplacian where we have used the definition of the potential $V(x)$. Proposition 4.1 shows that the gradient flow associated with \mathcal{D}_μ corresponds to an advection–diffusion equation with drift field ∇V . Equation (7) describes an advection-diffusion process: the first term on the r.h.s is an advection along the flow lines of ∇V whereas the second term is a regular diffusion process.

Equivalently, we can apply duality with respect to the standard $L^2(\Omega)$ scalar product. This yields the operator

$$\begin{aligned} \mathcal{D}_\mu(f, g) &= \frac{1}{2} \int_\Omega dx \mu(x) (\nabla g \cdot \nabla f) \\ &= -\frac{1}{2} \int_\Omega dx g (\nabla \mu \nabla f + \mu \Delta f) \\ &\equiv \int_\Omega dx g \tilde{L}_\mu f. \end{aligned}$$

where

$$\tilde{L}_\mu f = -\frac{1}{2}(\nabla \mu \nabla f + \mu \Delta f). \quad (8)$$

Thus, changing the scalar product changes the explicit form of the generator, while leaving the underlying Dirichlet form unchanged.

4.2. The Bakry–Emery Laplacian on Graphs

The formulation above isolates the role of the density μ in shaping transport dynamics, making it especially well suited for extension to discrete domains such as graphs. We will now construct the discrete equivalent of (8).

Proposition 4.2 (Closed form of the graph Bakry–Émery Laplacian). *Let $\mu : V \rightarrow \mathbb{R}_+$ and define the weighted Dirichlet form*

$$D_\mu^G(f, g) = \frac{1}{2} \sum_i \mu_i \sum_{j \sim i} \nabla_{ij}^G f \nabla_{ij}^G g \quad (9)$$

Then there exists a unique symmetric positive semidefinite matrix L_μ such that

$$D_\mu^G(f, g) = f^\top L_\mu g.$$

L_μ is a weighted graph Laplacian of the form $L_\mu = D_\mu - A_\mu$ where $A_\mu = M_\mu \odot A$, with \odot being the Hadamard product and $M_{ij}^\mu = \frac{1}{2}(\mu_i + \mu_j)$. The weighted adjacency matrix A^μ preserves the original adjacency and the corresponding degree matrix is defined as usual $D_\mu = \text{diag}(A_\mu \mathbf{1})$.

We note that we recover the combinatorial Laplacian when $\mu(i) = 1, \forall i$ and that we can use the new degree matrix D_μ to form a normalized Laplacian. A closer inspection also reveals that

$$(L_\mu f)_i = \mu_i L f(i) + \frac{1}{2} \sum_{j \sim i} \nabla_{ij}^G \mu \nabla_{ij}^G f \quad (10)$$

whereby the first term corresponds to an isotropic diffusion, while the second term couples discrete gradients of μ and f along edges. The second term biases diffusion depending on the relative variation of μ along each edge, thereby selecting preferred directions of transport. This can be interpreted as a discrete advection term, directly mirroring the geometry-induced drift present in the continuous operator (8). The advection-diffusion equation which occurs as the gradient flow of (9) has the simple form of a heat diffusion equation:

$$\frac{\partial f}{\partial t} = L_\mu f.$$

The corresponding BE-Laplacian has a well-behaved spectral decomposition and heat kernel. It can therefore be used as a simple plug-in replacement for the traditional graph Laplacian in any spectral GNN. Before doing so, we will first highlight some of its key characteristics.

4.3. Properties of the BE-Laplacian on Graphs

In this section, we present key spectral properties and foundational results showing how μ can be leveraged to adapt and control the propagation dynamics on the graph. To this end, we relate the spectra of L and L_μ through their Rayleigh quotients:

$$\mathcal{R}(f) = \frac{f^\top L f}{f^\top f} \quad \text{and} \quad \mathcal{R}_\mu(f) = \frac{f^\top L_\mu f}{f^\top f}.$$

Definition 4.3. Let $f \in \mathbb{R}^n$, we denote the squared euclidean norm of its local variation:

$$N(f) = \left(\frac{\|\nabla^G f(u)\|_2^2}{f^\top f} \right)_{u \in V} \in \mathbb{R}^n$$

where

$$\|\nabla^G f(u)\|_2^2 = \sum_{v \sim u} (f(u) - f(v))^2.$$

and the associated probability distribution

$$p_f = \frac{1}{\mathbf{1}^\top N(f)} N(f).$$

Lemma 4.4. *Let $f \in \mathbb{R}^n$, we have*

$$\mathcal{R}_\mu(f) = \|\mu\|_1 \mathbb{E}_\mu[p_f] \mathcal{R}(f),$$

where $\mathbb{E}_\mu[p_f]$ is the expectation of p_f under μ normalized to be a probability distribution.

This factorization isolates three key contributors to the spectrum of the BE-Laplacian L_μ : the global scaling determined by $\|\mu\|_1$; a local interaction between μ and p_f captured through the μ -weighted expectation $\mathbb{E}_\mu[p_f]$, and the spectral structure of the underlying combinatorial Laplacian as encoded by $\mathcal{R}(f)$. From this decomposition, we derive the following theorem.

Theorem 4.5. *Let $\lambda_0 = 0 \leq \lambda_1 \leq \dots \leq \lambda_{n-1}$ be the eigenvalues of L , and let λ_k^μ denote the eigenvalues of L_μ , ordered similarly. Let f_0, \dots, f_{n-1} and g_0, \dots, g_{n-1} be two orthonormal bases of eigenvectors associated with L . For all $k \in \{0, \dots, n-1\}$:*

$$\lambda_k \|\mu\|_1 m_g \leq \lambda_k^\mu \leq \lambda_k \|\mu\|_1 M_f$$

where

$$m_g = \min_{\substack{g \in \text{Span}(g_k, \dots, g_{n-1}) \\ \|g\|_2=1}} \mathbb{E}_\mu[p_g]$$

and

$$M_f = \max_{\substack{f \in \text{Span}(f_1, \dots, f_k) \\ \|f\|_2=1}} \mathbb{E}_\mu[p_f]$$

Since eigenvectors associated with low (resp. high) eigenvalues tend to concentrate their variations in sparse (resp. dense) regions of the graph, this formulation enables targeted spectral modulation by appropriately shaping μ , without relying on its global scale $\|\mu\|_1$. As corollaries, we show how to modulate the spectrum and the input-output sensitivity between a given pair of nodes on the star graph, only by tuning μ . This graph is interesting as it is a common example of bottleneck or articulating point between clusters. We further refer to $\frac{\mu}{\|\mu\|_1}$ as $\tilde{\mu}$.

Corollary 4.6. *Let μ be such that $\tilde{\mu}(1) = \tilde{\mu}(2) = 0$ and $\tilde{\mu}(k) = \frac{1}{n-2}$ for all $k \notin \{1, 2\}$, then:*

$$\lambda_1^\mu \leq \frac{1}{2(n-2)} \|\mu\|_1 \lambda_1.$$

Corollary 4.6 implies that one can strongly reduce the spectral gap by down-weighting just two nodes, without cutting the graph or changing its topology.

Corollary 4.7. *Let μ be such that*

$$\tilde{\mu}(u) = \begin{cases} \frac{1}{2} & \text{if } u = 0, \\ 0 & \text{if } u \in \{1, 2\}, \\ \frac{1}{2(n-1)} + \frac{1}{(n-1)(n-3)} & \text{else,} \end{cases}$$

and $\|\mu\|_1 = 2$, then simultaneously:

$$\frac{3}{2} \lambda_{n-1} \leq \lambda_{n-1}^\mu \quad \text{and} \quad \lambda_1^\mu \leq \frac{1}{2} \lambda_1.$$

Spectral Gap: Corollary 4.7 shows that node-wise modulation allows independent control of the spectral gap and the spectral radius while preserving connectivity and total diffusion strength. By reducing the spectral gap while preserving or increasing the spectral radius, the Bakry–Emery Laplacian slows excessive global mixing and redistributes flow away from bottleneck nodes. This directly mitigates over-squashing, as information is no longer forced through a small set of nodes but instead propagates along task-adaptive routes encoded by the learned potential. Proofs are detailed in the appendix. This is later experimentally validated in Figure 2 of Section 5.

In order to illustrate how the BE-Laplacian can correct weaknesses of spectral GNNs, let us consider a simple example. It has been shown in Lu et al. (2024) and later refined in Qin et al. (2025) that repeated Laplacian eigenvalues are detrimental to the expressive power of spectral GNNs. A simple way to understand this phenomenon is to realize that eigenspaces related to repeated eigenvalues are treated as one-dimensional, irrespective of their actual dimension.

We show on a simple example how a biased Laplacian can circumvent this problem. Consider a ring graph with 4 nodes. The corresponding spectrum is $S = \{0, 2, 2, 4\}$, with the first non-zero eigenvalue repeated. Now consider the potential $\mu[1] = \mu[2] = \mu[4] = 1$ and $\mu[3] = 3$. It is easy to compute that the spectrum of L_μ is now $S_\mu = \{0, \frac{1}{2}(9 - \sqrt{17}), 3, \frac{1}{2}(9 + \sqrt{17})\}$. The underlying adjacency has not changed, but the potential has broken the symmetry. In practice it is not trivial to manually construct a potential for large graphs or for targeting specific properties of the graph involved in solving a machine learning task. In the next section, we propose a neural parameterization of μ and leverage the corresponding Laplacian to create a new class of spectral GNNs with adaptive aggregation mechanism.

4.4. A novel class of spectral GNNs

The explicit form of the BE-Laplacian that was derived in Section 4.2 has exactly the form of the combinatorial Laplacian and can therefore be used in any spectral GNN, with minimal modification to the architecture. As discussed in Section 4.3 the advection potential μ controls the properties

of L_μ but it can be very difficult in practice to design this potential by hand. We therefore propose a 2-steps strategy. First, we make a neural parameterization of μ . This can be realized in many ways, but in practice we will use a simple but sufficiently expressive GCN: $\mu = GCN(A, \Theta)$ where A is the original adjacency matrix and Θ stands for all learnable parameters of the network. We chose this neural parameterization because of its structural bias. The second step is to construct L_μ and use it directly into a downstream spectral μ -GNN. This leads to a new family of architectures, with varying parameterization of μ and downstream GNN that can be learned end to-end to solve a given task. At training time, the potential μ will be adapted so the downstream μ -GNN solves the task and will thus depend on the task and distribution of training samples. As we shall see below, inspecting μ as a graph signal reveals much about the strategy employed by the network.

μ -ChebNet Filter: After parameterizing the potential μ and thus learning the associated Laplacian L_μ , we may incorporate it into an architecture that is particularly well suited to this setting, since its formulation depends only on the Laplacian operator: the ChebNet model (Defferrard et al., 2016).

Stable variant: A variant architecture particularly well suited to the μ -Laplacian is the *Stable-ChebNet* also discussed in Section 3.2. The node update rule for Stable-ChebNet is defined as follows:

$$X^{(l+1)} = X^{(l)} + \epsilon \left(\sum_{k=0}^K T_k(L) X^{(l)} (W_k - W_k^T - \gamma I) \right)$$

Here, I denotes the identity matrix, $\gamma \in \mathbb{R}$ is a hyperparameter and $\epsilon \in \mathbb{R}^+$ represents the step size of the discretization. We refer to Theorem 3 of (Hariri et al., 2025) to show that the μ -Stable ChebNet retains purely imaginary eigenvalues and therefore remains stable.

5. Experiments

We evaluate our method across a spectrum of benchmarking tasks that probe both synthetic and real-world graph reasoning. The Barbell dataset introduced in (Bamberger et al., 2024) comprises synthetic graphs with two dense cliques connected by a narrow bridge, designed to stress long-range propagation and oversquashing; success on this benchmark indicates effective transmission of information across structural bottlenecks. Moreover, we test our model on the Graph Property Prediction benchmark from (Corso et al., 2020) which consists of both graph and node-level classification. The goal is to predict structural quantities (e.g., diameter, eccentricity) from graph topology and features by aggregating information over large receptive fields.

Finally, ogbn-proteins is a large-scale real-world dataset from the Open Graph Benchmark (Hu et al., 2020) that contains protein–protein association graphs with multi-label targets, and is commonly used to evaluate scalability and generalization of graph models on biologically relevant, densely connected graphs.

Discussion: Across these benchmarks, μ -ChebNet consistently improves over previous spectral models. In the barbell oversquashing experiment (Table 2), μ -ChebNet achieves near-zero error even as graph size and depth increase, whereas ChebNet degrades and Stable-ChebNet only partially mitigates the issue. Since the topology is unchanged, this directly supports our theory that learning the node-wise potential μ reshapes the Laplacian spectrum to relieve bottlenecks without rewiring, showing that adaptive spectral geometry alone can restore long-range signal propagation.

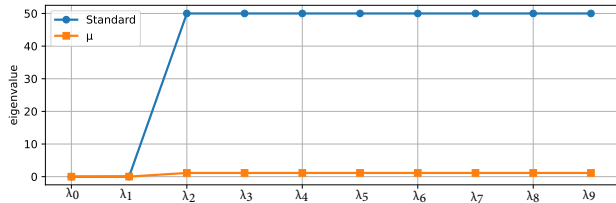


Figure 2. Eigenvalue distribution comparison on the Barbell task using the standard normalized Laplacians vs μ -Laplacian

On graph property prediction (Table 1), μ -ChebNet systematically improves over ChebNet and is further strengthened when combined with stability constraints. Stabilization operates at the level of the weights, constraining the training dynamics across hops, but leaves the underlying graph operator unchanged. In contrast, μ acts directly on the Laplacian itself, modifying the geometry that governs information flow. Adaptive geometry and dynamical stability are complementary: stability controls how far information can propagate, while μ controls where it propagates.

On ogbn-proteins (Table 3), μ -ChebNet matches strong spectral baselines and remains competitive with transformer models despite using no global attention. Together with the structure of the learned potentials, which concentrate along efficient communication paths, this indicates that μ acts as a global routing field steering diffusion in a task-dependent manner. This hybrid behavior bridges message-passing adaptivity and spectral efficiency: the model learns propagation geometry during training but retains a fixed operator at inference, offering a principled alternative to attention and graph rewiring. Finally, Figure 2 shows the normalized Laplacian spectra of barbell graphs. Whereas the standard operator exhibits a pronounced spectral gap, leading to rapid representation collapse, the introduction of the learned potential regularizes the spectrum and alleviates

Table 1. Mean test set $\log_{10}(\text{MSE})$ and standard deviation averaged over 4 random weight initializations for each configuration on the Graph Property Prediction dataset. The lower the better.

Model	Diameter	SSSP	Eccentricity
GCN	0.7424 ± 0.0466	0.9499 ± 0.0001	0.8468 ± 0.0028
GAT	0.8221 ± 0.0752	0.6951 ± 0.1499	0.7909 ± 0.0222
GraphSAGE	0.8645 ± 0.0401	0.2863 ± 0.1843	0.7863 ± 0.0207
GIN	0.6131 ± 0.0990	-0.5408 ± 0.4193	0.9504 ± 0.0007
GCNII	0.5287 ± 0.0570	-1.1329 ± 0.0135	0.7640 ± 0.0355
DGC	0.6028 ± 0.0050	0.1483 ± 0.0231	0.8261 ± 0.0032
GRAND	0.6715 ± 0.0490	-0.0942 ± 0.3897	0.6602 ± 0.1393
A-DGN w/ GCN backbone	0.2271 ± 0.0804	-1.8288 ± 0.0607	0.7177 ± 0.0345
ChebNet	-0.1517 ± 0.0343	-1.8519 ± 0.0539	-1.2151 ± 0.0852
Stable-ChebNet	-0.2477 ± 0.0526	-2.2111 ± 0.0160	-2.1043 ± 0.0766
mu-ChebNet (ours)	-0.2075 ± 0.0634	-2.3149 ± 0.0301	-1.8740 ± 0.0597
+Stability	-0.3179 ± 0.0182	-2.3217 ± 0.0330	-2.0338 ± 0.0571

Method	K	50	70
ChebNet	$K = 9$	0.32 ± 0.39	1.08 ± 0.05
	$K = 10$	0.05 ± 0.00	1.08 ± 0.01
Stable-ChebNet	$K = 9$	0.17 ± 0.11	0.47 ± 0.49
	$K = 10$	0.05 ± 0.00	0.06 ± 0.03
mu-ChebNet	$K = 9$	0.03 ± 0.01	0.02 ± 0.02
	$K = 10$	0.03 ± 0.01	0.02 ± 0.02

Method	K	100
ChebNet	$K = 20$	0.87 ± 0.05
Stable-ChebNet	$K = 20$	0.21 ± 0.27
mu-ChebNet (ours)	$K = 15$	0.02 ± 0.01

Table 2. Mean squared error (MSE) of ChebNet variants on the over-squashing experiment for barbell graphs. Up: sizes $N = 50, 70$ for $K = 9$ and 10. Down: size $N = 100$ for $K = 20$.

this effect. This is consistent with our theoretical analysis (see Section 4.3). Appendix B.4 provides another example of visualizing the potential as a way to explain the neural net’s performance.

6. Conclusion

We introduced a novel graph Laplacian inspired by Bakry–Émery theory that integrates diffusion and advection through a learnable node-wise potential. This operator enables fine-grained control of propagation dynamics while preserving graph topology and can be seamlessly incorporated into spectral GNN architectures. This allows improved long-range information propagation within the graph. Our theoretical analysis highlights how the potential modulates the spectrum, bridging the gap between message-

Table 3. Accuracy on the ogbn-proteins dataset.

Model	Accuracy (%)
MLP	72.04 ± 0.48
GCN	72.51 ± 0.35
ChebNet	77.55 ± 0.43
SGC	70.31 ± 0.23
GCN-NSAMPLER	73.51 ± 1.31
GAT-NSAMPLER	74.63 ± 1.24
SIGN	71.24 ± 0.46
NodeFormer	77.45 ± 1.15
SGFormer	79.53 ± 0.38
SPEXPFORMER	80.65 ± 0.07
Stable-ChebNet	79.55 ± 0.34
mu-ChebNet (ours)	79.36 ± 0.41

passing and spectral approaches. Building on this insight, we proposed μ -ChebNet, which jointly learns the potential and spectral filters. Extensive experiments demonstrate that these architectures outperform strong baselines, mitigate oversquashing, and provide interpretable attention-like mechanisms. Looking ahead, we believe the Bakry–Émery Laplacian opens new directions for graph machine learning beyond node representation learning. Future work will explore its role in tasks such as graph clustering, community detection, and controllable diffusion processes, as well as its integration into dynamic graph settings. By leveraging its theoretical foundations, we aim to develop a broader class of models that combine interpretability, adaptability, and efficiency.

Impact Statement

This work advances the theoretical foundations of graph machine learning by introducing a principled operator that unifies diffusion and advection on graphs. Beyond improving predictive performance and interpretability in GNNs, the proposed Bakry–Émery Laplacian offers a flexible framework for controlling information flow without altering graph topology. Potential applications extend to clustering, community detection, and dynamic graph analysis, enabling more robust and transparent models for domains such as social networks, biological systems, and scientific simulations. While our approach is primarily methodological, future work should consider fairness and bias implications when learning potentials on sensitive graphs.

Code Availability

The full source code will be released upon acceptance of the paper.

Acknowledgments

V. K.-B. and M. Z. are funded by the Swiss National Science Foundation, Grant Number 10003660.

References

- Alon, U. and Yahav, E. On the bottleneck of graph neural networks and its practical implications. In *International Conference on Learning Representations*, 2021.
- Arnaiz-Rodríguez, A. and Errica, F. Oversmoothing, Oversquashing, Heterophily, Long-Range, and more: Demystifying Common Beliefs in Graph Machine Learning, June 2025. URL <http://arxiv.org/abs/2505.15547>. arXiv:2505.15547 [cs].
- Arnaiz-Rodríguez, A., Begga, A., Escolano, F., and Oliver, N. Diffwire: Inductive graph rewiring via the lov^{as} bound. *arXiv preprint arXiv:2206.07369*, 2022.
- Arroyo, Á., Gravina, A., Gutteridge, B., Barbero, F., Gallicchio, C., Dong, X., Bronstein, M., and Vandergheynst, P. On vanishing gradients, over-smoothing, and oversquashing in gnn: Bridging recurrent and graph learning. *arXiv preprint arXiv:2502.10818*, 2025.
- Attali, H., Buscaldi, D., and Pernelle, N. Rewiring techniques to mitigate oversquashing and oversmoothing in gnn: A survey. *arXiv preprint arXiv:2411.17429*, 2024.
- Bakry, D., Gentil, I., and Ledoux, M. *Analysis and geometry of Markov diffusion operators*, volume 348. Springer Science & Business Media, 2013.
- Bakry, D. and Émery, M. Diffusions hypercontractives. In *Séminaire de Probabilités, XIX, 1983/84*, volume 1123 of *Lecture Notes in Math.*, pp. 177–206. Springer, Berlin, 1985. ISBN 978-3-540-15230-9. doi: 10.1007/BFb0075847.
- Bamberger, J., Barbero, F., Dong, X., and Bronstein, M. Bundle neural networks for message diffusion on graphs. *arXiv preprint arXiv:2405.15540*, 2024.
- Battaglia, P. W., Hamrick, J. B., Bapst, V., Sanchez-Gonzalez, A., Zambaldi, V., Malinowski, M., Tacchetti, A., Raposo, D., Santoro, A., Faulkner, R., et al. Relational inductive biases, deep learning, and graph networks. *arXiv preprint arXiv:1806.01261*, 2018.
- Bo, D., Shi, C., Wang, L., and Liao, R. Specformer: Spectral graph neural networks meet transformers. *arXiv preprint arXiv:2303.01028*, 2023.
- Bruna, J., Zaremba, W., Szlam, A., and LeCun, Y. Spectral networks and locally connected networks on graphs. *arXiv preprint arXiv:1312.6203*, 2013.
- Chamberlain, B., Rowbottom, J., Eynard, D., Di Giovanni, F., Dong, X., and Bronstein, M. Beltrami flow and neural diffusion on graphs. *Advances in Neural Information Processing Systems*, 34:1594–1609, 2021a.
- Chamberlain, B. P., Rowbottom, J., Gorinova, M., Webb, S., Rossi, E., and Bronstein, M. M. GRAND: Graph neural diffusion. In *International Conference on Machine Learning (ICML)*, pp. 1407–1418. PMLR, 2021b.
- Chen, J., Gao, K., Li, G., and He, K. Nagphormer: A tokenized graph transformer for node classification in large graphs. *arXiv preprint arXiv:2206.04910*, 2022.
- Chen, M., Wei, Z., Huang, Z., Ding, B., and Li, Y. Simple and Deep Graph Convolutional Networks. In III, H. D. and Singh, A. (eds.), *Proceedings of the 37th International Conference on Machine Learning*, volume 119 of *Proceedings of Machine Learning Research*, pp. 1725–1735. PMLR, 13–18 Jul 2020.
- Chung, F. R. *Spectral graph theory*, volume 92. American Mathematical Soc., 1997.
- Corso, G., Cavalleri, L., Beaini, D., Liò, P., and Veličković, P. Principal neighbourhood aggregation for graph nets. In *Advances in Neural Information Processing Systems (NeurIPS)*, volume 33, pp. 13260–13271, 2020.
- Defferrard, M., Bresson, X., and Vandergheynst, P. Convolutional neural networks on graphs with fast localized spectral filtering. *Advances in neural information processing systems*, 29, 2016.

- Frasca, F., Rossi, E., Eynard, D., Chamberlain, B., Bronstein, M., and Monti, F. Sign: Scalable inception graph neural networks. *arXiv preprint arXiv:2004.11198*, 2020.
- Gilmer, J., Schoenholz, S. S., Riley, P. F., Vinyals, O., and Dahl, G. E. Neural message passing for quantum chemistry. In *International conference on machine learning*, pp. 1263–1272. PMLR, 2017.
- Gravina, A., Bacciu, D., and Gallicchio, C. Anti-Symmetric DGN: a stable architecture for Deep Graph Networks. In *The Eleventh International Conference on Learning Representations*, 2023.
- Hamilton, W., Ying, Z., and Leskovec, J. Inductive representation learning on large graphs. *Advances in neural information processing systems*, 30, 2017.
- Hariri, A., Arroyo, Á., Gravina, A., Eliasof, M., Schönlieb, C.-B., Bacciu, D., Azzadenesheli, K., Dong, X., and Vandergheynst, P. Return of ChebNet: Understanding and Improving an Overlooked GNN on Long Range Tasks, October 2025. arXiv:2506.07624 [cs].
- He, X., Hooi, B., Laurent, T., Perold, A., LeCun, Y., and Bresson, X. A generalization of vit/mlp-mixer to graphs. In *International conference on machine learning*, pp. 12724–12745. PMLR, 2023.
- Hu, W., Fey, M., Zitnik, M., Dong, Y., Ren, H., Liu, B., Catasta, M., and Leskovec, J. Open graph benchmark: datasets for machine learning on graphs. In *Proceedings of the 34th International Conference on Neural Information Processing Systems, NIPS '20*. Curran Associates Inc., 2020. ISBN 9781713829546.
- Jin, Y. and Zhu, X. Oversmoothing alleviation in graph neural networks: a survey and unified view: Y. jin, x. zhu. *Knowledge and Information Systems*, 67(12):11259–11285, 2025.
- Kipf, T. N. and Welling, M. Semi-Supervised Classification with Graph Convolutional Networks, February 2017. arXiv:1609.02907 [cs].
- Levie, R., Huang, W., Bucci, L., Bronstein, M., and Kutyniok, G. Transferability of spectral graph convolutional neural networks. *J. Mach. Learn. Res.*, 22(1), January 2021. ISSN 1532-4435.
- Li, Q., Han, Z., and Wu, X.-M. Deeper insights into graph convolutional networks for semi-supervised learning. In *AAAI Conference on Artificial Intelligence*, volume 32, 2018.
- Lu, K., Yu, Y., Fei, H., Li, X., Yang, Z., Guo, Z., Liang, M., Yin, M., and Chua, T.-S. Improving Expressive Power of Spectral Graph Neural Networks with Eigenvalue Correction, 2024. URL <http://arxiv.org/abs/2401.15603>.
- Poli, M., Massaroli, S., Park, J., Yamashita, A., Asama, H., and Park, J. Graph neural ordinary differential equations. *arXiv preprint arXiv:1911.07532*, 2019.
- Qin, T., Chen, K.-J., and Liu, Z. Enhancing Spectral GNNs: From Topology and Perturbation Perspectives. 2025. URL <https://openreview.net/forum?id=OjIMyKYviK¬eId=7fwhJOe1JU>.
- Rampášek, L., Galkin, M., Dwivedi, V. P., Luu, A. T., Wolf, G., and Beaini, D. Recipe for a general, powerful, scalable graph transformer. *Advances in Neural Information Processing Systems*, 35:14501–14515, 2022.
- Rusch, T. K., Bronstein, M. M., and Mishra, S. A Survey on Oversmoothing in Graph Neural Networks. *arXiv preprint arXiv:2303.10993*, 2023.
- Scarselli, F., Gori, M., Tsoi, A. C., Hagenbuchner, M., and Monfardini, G. The graph neural network model. *IEEE transactions on neural networks*, 20(1):61–80, 2008.
- Shao, Z., Shi, D., Han, A., Guo, Y., Zhao, Q., and Gao, J. Unifying over-smoothing and over-squashing in graph neural networks: A physics informed approach and beyond. *arXiv preprint arXiv:2309.02769*, 2023.
- Shi, Y., Huang, Z., Feng, S., Zhong, H., Wang, W., and Sun, Y. Masked label prediction: Unified message passing model for semi-supervised classification. In *Proceedings of the Thirtieth International Joint Conference on Artificial Intelligence*, pp. 1548–1554. International Joint Conferences on Artificial Intelligence Organization, 2021.
- Shirzad, H., Vellingker, A., Venkatachalam, B., Sutherland, D. J., and Sinop, A. K. Exphormer: Sparse transformers for graphs. In *International Conference on Machine Learning*, pp. 31613–31632. PMLR, 2023.
- Shirzad, H., Lin, H., Venkatachalam, B., Vellingker, A., Woodruff, D. P., and Sutherland, D. J. Even sparser graph transformers. *Advances in Neural Information Processing Systems*, 37:71277–71305, 2024.
- Veličković, P., Cucurull, G., Casanova, A., Romero, A., Lio, P., and Bengio, Y. Graph attention networks. In *Proceedings of the International Conference on Learning Representations (ICLR)*, 2018.
- Wang, Y., Wang, Y., Yang, J., and Lin, Z. Dissecting the Diffusion Process in Linear Graph Convolutional Networks. In *Advances in Neural Information Processing Systems*, volume 34, pp. 5758–5769. Curran Associates, Inc., 2021.

- Wang, Z., Cerviño, J., and Ribeiro, A. Generalization of graph neural networks is robust to model mismatch. In *Proceedings of the AAAI Conference on Artificial Intelligence*, volume 39, pp. 21402–21410, 2025.
- Wu, Q., Zhao, W., Li, Z., Wipf, D. P., and Yan, J. Nodeformer: A scalable graph structure learning transformer for node classification. *Advances in Neural Information Processing Systems*, 35:27387–27401, 2022.
- Wu, Q., Yang, C., Zeng, K., Nie, F., Bronstein, M., and Yan, J. Advective diffusion transformers for topological generalization in graph learning. *arXiv preprint arXiv:2310.06417*, 2023a.
- Wu, Q., Zhao, W., Yang, C., Zhang, H., Nie, F., Jiang, H., Bian, Y., and Yan, J. Sgformer: Simplifying and empowering transformers for large-graph representations. *Advances in Neural Information Processing Systems*, 36: 64753–64773, 2023b.
- Wu, Q., Wipf, D., and Yan, J. Transformers from diffusion: A unified framework for neural message passing. *Journal of Machine Learning Research*, 26(129):1–47, 2025a.
- Wu, Q., Yang, C., Zeng, K., and Bronstein, M. M. Supercharging graph transformers with advective diffusion. In *Forty-second International Conference on Machine Learning*, 2025b.
- Xu, K., Hu, W., Leskovec, J., and Jegelka, S. How powerful are graph neural networks? In *International Conference on Learning Representations (ICLR)*, 2019.
- Zeng, H., Zhou, H., Srivastava, A., Kannan, R., and Prasanna, V. Graphsaint: Graph sampling based inductive learning method. *arXiv preprint arXiv:1907.04931*, 2019.

A. Proofs

Proposition 4.1

Proof. We define $f, g : \Omega \subset \mathbb{R}^d \rightarrow \mathbb{R}$, with Ω being any smooth region with boundary $\partial\Omega$, such that f, g vanish on $\partial\Omega$. We first recall the Dirichlet (symmetric) bi-linear form $\mathcal{D}(f, g)$ defined as:

$$\mathcal{D}(f, g) = \frac{1}{2} \int_{\Omega} dx (\nabla g \cdot \nabla f) \quad (11)$$

and there exists a unique symmetric, positive-definite operator L such that

$$\mathcal{D}(f, g) = \int_{\Omega} dx g Lf = \int_{\Omega} dx f Lg.$$

Integrating by part and using boundary conditions on f and g , the expression of $\mathcal{D}(f, g)$ shows that L is proportional to the Laplacian Δ on Ω :

$$\mathcal{D}(f, g) = -\frac{1}{2} \int_{\Omega} dx g \Delta f \Rightarrow L = -\frac{1}{2} \Delta.$$

We now define an integrable, non-negative density function $\mu : \Omega \rightarrow \mathbb{R}^+$, by $\mu(x) = Z^{-1} e^{-V(x)}$ where V is a suitable function we shall denote by the term potential below and Z a normalizing constant. Without associating too much interpretation to its actual form, we will use $\mu(x)$ to weight the Lebesgue measure in (5) and define a weighted Dirichlet form $\mathcal{D}_{\mu}(f, g)$ as

$$\mathcal{D}_{\mu}(f, g) = \frac{1}{2} \int_{\Omega} dx \mu(x) (\nabla g \cdot \nabla f). \quad (12)$$

Similarly to (5), \mathcal{D}_{μ} defines a symmetric positive-definite operator L_{μ} :

$$\begin{aligned} \mathcal{D}_{\mu}(f, g) &= \frac{1}{2} \int_{\Omega} dx \mu(x) (\nabla g \cdot \nabla f) \\ &= -\frac{1}{2} \int_{\Omega} dx \mu(x) \left(g \frac{\nabla \mu}{\mu} \cdot \nabla f + g \Delta f \right) \\ &= -\frac{1}{2} \int_{\Omega} dx \mu(x) g \left(\nabla \log(\mu) \cdot \nabla f + \Delta f \right) \\ &\equiv \int_{\Omega} dx \mu(x) g L_{\mu} f. \end{aligned}$$

We therefore recover the Bakry-Emery Laplacian:

$$L_{\mu} f = -\frac{1}{2} \left(\nabla \log(\mu) \cdot \nabla f + \Delta f \right) \quad (13)$$

$$= \frac{1}{2} \nabla V \cdot \nabla f - \frac{1}{2} \Delta f, \quad (14)$$

where we have used the definition of the potential $V(x)$. Equation (14) describes an advection-diffusion process: the first term on the r.h.s is an advection along the flow lines of ∇V whereas the second term is a regular diffusion process.

Equivalently, we can apply duality with respect to the standard $L^2(\Omega)$ scalar product. This yields the operator

$$\begin{aligned} \mathcal{D}_{\mu}(f, g) &= \frac{1}{2} \int_{\Omega} dx \mu(x) (\nabla g \cdot \nabla f) \\ &= -\frac{1}{2} \int_{\Omega} dx g (\nabla \mu \nabla f + \mu \Delta f) \\ &\equiv \int_{\Omega} dx g \tilde{L}_{\mu} f. \end{aligned}$$

where

$$\tilde{L}_{\mu} f = -\frac{1}{2} (\nabla \mu \nabla f + \mu \Delta f) \quad (15)$$

Thus, changing the scalar product changes the explicit form of the generator, while leaving the underlying Dirichlet form unchanged. \square

Proposition 4.2

Proof. We first consider a non-negative node-wise weight $\mu : V \rightarrow \mathbb{R}^+$ and the corresponding Dirichlet bilinear form:

$$\mathcal{D}_\mu^G(f, g) = \frac{1}{2} \sum_i \mu_i \sum_{j \sim i} \nabla_{ij}^G f \nabla_{ij}^G g. \quad (16)$$

The symmetry with (12) reveals that the Dirichlet form is a weighted scalar product of the components of the graph gradients of f and g at each node. Again, there exists a unique symmetric positive-definite matrix L_μ such that $\mathcal{D}_\mu^G(f, g) = f^T L_\mu g = (L_\mu f)^T g$. Developing \mathcal{D}_μ^G we get:

$$\begin{aligned} \mathcal{D}_\mu^G(f, g) &= \frac{1}{2} \sum_i \mu_i \sum_{j \sim i} \nabla_{ij}^G f \nabla_{ij}^G g \\ &= \frac{1}{2} \sum_i \mu_i \sum_{j \sim i} (g(i) - g(j))(f(i) - f(j)) \\ &= \frac{1}{2} \sum_i \sum_{j \sim i} \frac{\mu_i S_{ij} + \mu_j S_{ji}}{2} \\ &= \frac{1}{2} \sum_i \sum_{j \sim i} \frac{S_{ij}(\mu_i + \mu_j)}{2} \\ &= \sum_{i \sim j} \frac{\mu_i + \mu_j}{2} (f(i) - f(j))(g(i) - g(j)) \\ &= \frac{1}{2} \sum_i \sum_j A_{\mu, ij} (f(i) - f(j))(g(i) - g(j)) \\ &= \frac{1}{2} \sum_i \sum_j g(i) A_{\mu, ij} (f(i) - f(j)) - g(j) A_{\mu, ij} (f(i) - f(j)) \\ &= \frac{1}{2} \sum_i \sum_j g(i) A_{\mu, ij} (f(i) - f(j)) - g(i) A_{\mu, ji} (f(j) - f(i)) \\ &= \sum_i \sum_j g(i) A_{\mu, ij} (f(i) - f(j)) \\ &= \sum_i g(i) \left(D_{\mu, ii} f(i) - \sum_{j \sim i} A_{\mu, ij} f(j) \right) \end{aligned}$$

where we have defined $A_\mu = M_\mu \odot A$, with \odot being the Hadamard product and $M_{\mu, ij} = \frac{1}{2}(\mu_i + \mu_j)$. On line 3, we have defined $S_{ij} = (f(i) - f(j))(g(i) - g(j))$. On line 4, we use the symmetry property of the matrix S . A similar reasoning has been used on line 8, since $A_{\mu, ij}$ is also symmetric. The weighted adjacency matrix A_μ preserves the original adjacency and the corresponding degree matrix is defined as usual $D_\mu = \text{diag}(A_\mu \mathbf{1})$. Finally, we immediately see that:

$$D_\mu^G(f, g) = (L_\mu f)^T g \Rightarrow L_\mu = D_\mu - A_\mu \quad (17)$$

Which allows us to just simply compute A_μ and D_μ . \square

Derivation of Equation (10) We derive the decomposition of L_μ :

$$\begin{aligned} (L_\mu f)_i &= \sum_{j \sim i} \left(\mu_i - \frac{\mu_i - \mu_j}{2} \right) (f(j) - f(i)) \\ &= \mu_i \sum_{j \sim i} \nabla_{ij}^G f + \frac{1}{2} \sum_{j \sim i} \nabla_{ij}^G \mu \nabla_{ij}^G f \\ &= \mu_i L f(i) + \frac{1}{2} \sum_{j \sim i} \nabla_{ij}^G \mu \nabla_{ij}^G f \end{aligned}$$

Lemma 4.4

Proof. We simply write:

$$\mathcal{R}_\mu(f) = \frac{1}{2} \mu^\top \cdot N(f) = \|\mu\|_1 \left(\frac{1}{\|\mu\|_1} \mu^\top \cdot p_f \right) \cdot \frac{1}{2} (\mathbf{1}^\top \cdot N(f)) = \|\mu\|_1 \mathbb{E}_\mu[p_f] \mathcal{R}(f).$$

□

Theorem 4.5

Proof. We only prove the upper bound as the same reasoning applies to the lower bound. Let's define the set of euclidian subspaces of \mathbb{R}^n ,

$$\mathcal{F}_k = \{F, \dim(F) = k + 1 \text{ and } \lambda_k = \max \{ \mathcal{R}(f) \mid f \in F, \|f\|_2 = 1 \} \}$$

and fix $F \in \mathcal{F}_k$. By lemma 5.0.1

$$\begin{aligned} \max_{\substack{f \in F \\ \|f\|_2=1}} \mathcal{R}_\mu(f) &= \max_{\substack{f \in F \\ \|f\|_2=1}} \|\mu\|_1 \mathbb{E}_\mu[p_f] \mathcal{R}(f) \\ &\leq \|\mu\|_1 \left(\max_{\substack{f \in F \\ \|f\|_2=1}} \mathbb{E}_\mu[p_f] \right) \left(\max_{\substack{f \in F \\ \|f\|_2=1}} \mathcal{R}(f) \right) = \lambda_k \|\mu\|_1 \max_{\substack{f \in F \\ \|f\|_2=1}} \mathbb{E}_\mu[p_f]. \end{aligned}$$

Thus

$$\min_{F \in \mathcal{F}_{k+1}} \max_{\substack{f \in F \\ \|f\|_2=1}} \mathcal{R}_\mu(f) \leq \lambda_k \|\mu\|_1 \min_{F \in \mathcal{F}_{k+1}} \max_{\substack{f \in F \\ \|f\|_2=1}} \mathbb{E}_\mu[p_f].$$

And

$$\min_{\substack{F \subset \mathbb{R}^n \\ \dim(F)=k+1}} \max_{\substack{f \in F \\ \|f\|_2=1}} \mathcal{R}_\mu(f) \leq \min_{F \in \mathcal{F}_{k+1}} \max_{\substack{f \in F \\ \|f\|_2=1}} \mathcal{R}_\mu(f),$$

where

$$\min_{\substack{F \subset \mathbb{R}^n \\ \dim(F)=k+1}} \max_{\substack{f \in F \\ \|f\|_2=1}} \mathcal{R}_\mu(f) = \lambda_k^\mu$$

by the min-max theorem. □

Corollary 4.6

Proof. Let us consider λ_1^μ , the spectral gap of L_μ . The right-hand side of the previous inequality reads:

$$\lambda_1^\mu \leq \lambda_1 \|\mu\|_1 \mathbb{E}_\mu[p_{f_1}],$$

where f_1 is an eigenvector of L associated with λ_1 .

Let S_n be the star graph with one central node u_0 connected to $n - 1$ leaves. The standard Laplacian L of S_n has eigenvalues:

- $\lambda_0 = 0$ (constant eigenvector),
- $\lambda_1 = 1$ (multiplicity $n - 2$),
- $\lambda_{n-1} = n$ (associated to the central node's variation).

The eigenspace of λ_1 is spanned by the basis $\{f_i\}_{i \in \{1, \dots, n-2\}}$, defined by:

$$f_i(j) = \begin{cases} \frac{1}{\sqrt{2}} & \text{if } j = 1, \\ -\frac{1}{\sqrt{2}} & \text{if } j = i + 1, \\ 0 & \text{else.} \end{cases}$$

These vectors all have unit norm but are not orthogonal. However, since our analysis only involves f_1 independently of the others, there is no need to modify it. Thus

$$\|\nabla f_1(u)\|_2^2 = \begin{cases} 1 & \text{if } u = 0, \\ \frac{1}{2} & \text{if } u = 1, \\ \frac{1}{2} & \text{if } u = 2, \\ 0 & \text{else,} \end{cases}$$

and

$$p_{f_1}(u) = \begin{cases} \frac{1}{2} & \text{if } u = 0, \\ \frac{1}{4} & \text{if } u \in \{1, 2\}, \\ 0 & \text{else.} \end{cases}$$

Setting $\mu(0) = \mu(1) = \mu(2) = 0$ and $\mu(k) = \frac{1}{n-3}$ for all $k \in \{3, \dots, n-1\}$ might appear effective for reducing the spectral gap, but it actually forces $\lambda_1^\mu = 0$, since the edges u_0u_1 and u_0u_2 are effectively removed—disconnecting the graph. It is easy to imagine how this could be undesirable, as our interest in the star graph stems from its role as a common bridge between distinct clusters in large graphs.

A safer and still effective alternative is to set only $\mu(1) = \mu(2) = 0$ and $\mu(k) = \frac{1}{n-2}$ elsewhere. Indeed, using our bound one can verify that the spectral gap of L_μ now satisfies:

$$\lambda_1^\mu \leq \frac{\lambda_1}{2(n-2)} \|\mu\|_1,$$

while the connectivity is preserved and the norm of μ remains unchanged. In this case, the link between nodes u_1, u_2 , and the rest of the graph is weakened rather than cut, reducing the flow of heat between potential associated clusters without fully isolating them. \square

Corollary 4.7

Proof. As the left-hand side of our inequality becomes:

$$\lambda_{n-1} \|\mu\|_1 \mathbb{E}_\mu[p_{g_{n-1}}] \leq \lambda_{n-1}^\mu,$$

where g_{n-1} is a unit-norm eigenvector of L associated with λ_{n-1} , given by:

$$g_{n-1}(u) = \begin{cases} \sqrt{\frac{n-1}{n}} & \text{if } u = 0, \\ -\frac{1}{\sqrt{n(n-1)}} & \text{else.} \end{cases}$$

From this, the local variation's norm vector becomes:

$$\|\nabla g_{n-1}(u)\|_2^2 = \begin{cases} \frac{n-1}{n} \left(\sqrt{n-1} + \frac{1}{\sqrt{n-1}} \right)^2 & \text{if } u = 0, \\ \frac{1}{n} \left(\sqrt{n-1} + \frac{1}{\sqrt{n-1}} \right)^2 & \text{else,} \end{cases}$$

implying:

$$p_{g_{n-1}}(u) = \begin{cases} \frac{1}{2} & \text{if } u = 0, \\ \frac{1}{2(n-1)} & \text{else.} \end{cases}$$

We now design a distribution μ to simultaneously reduce the spectral gap and increase the spectral radius:

$$\mu(u) = \begin{cases} \frac{1}{2} & \text{if } u = 0, \\ 0 & \text{if } u \in \{1, 2\}, \\ \frac{1}{2(n-1)} + \frac{1}{(n-1)(n-3)} & \text{else.} \end{cases}$$

Using our lower bound:

$$\frac{3}{4}\lambda_{n-1}\|\mu\|_1 \leq \lambda_{n-1}^\mu,$$

and

$$\lambda_1^\mu \leq \frac{\lambda_1}{4}\|\mu\|_1.$$

Hence, taking $\|\mu\|_1 = 2$ yields simultaneously:

$$\frac{3}{2}\lambda_{n-1} \leq \lambda_{n-1}^\mu \quad \text{and} \quad \lambda_1^\mu \leq \frac{\lambda_1}{2},$$

allowing us to both decrease the spectral gap and increase the spectral radius. Additionally, one can still multiply μ by a scaling factor—to modify the global diffusion rate for instance. \square

This example illustrates how modulating the node-wise diffusion rates via μ allows for flexible control over the spectral properties of a graph, without altering the underlying topology. The graph is never rewired, preserving its structure and connectivity.

B. Dataset and Baseline Description

B.1. Graph Property Prediction Tasks

We study a graph property prediction benchmark composed of three tasks that require reasoning over shortest-path distances at both the graph and node levels. Because shortest-path-based objectives inherently require information to propagate across large portions of a graph, this benchmark provides a natural stress test for evaluating the long-range modeling capabilities of graph neural networks. The *diameter* task is graph-level and aims to predict the maximum shortest-path distance between any two nodes, requiring global aggregation across distant regions of the graph. The *single-source shortest path (SSSP)* task is node-level and involves predicting each node’s shortest-path distance to a designated source node, placing strong emphasis on multi-hop information propagation. The *eccentricity* task is also node-level and requires predicting, for each node u , the maximum shortest-path distance between u and any other node. All three tasks depend critically on modeling long-range relationships within the graph.

The dataset contains 5,120 graphs for training, 640 for validation, and 1,280 for testing, using the same data splits and random seed as in (Gravina et al., 2023). Models are trained by minimizing mean squared error (MSE) for each task, with hyperparameters such as learning rate, weight decay, and number of layers selected via grid search. Each experiment is repeated with four random initializations, and results are reported as averages.

B.2. Barbell Graph Task Description

A barbell graph $B_{n,k}$ consists of two complete graphs K_n (referred to as the *bells*) connected by a simple path of length k (the *bridge*). Nodes within each bell exhibit dense intra-cluster connectivity, each having degree $n - 1$, while nodes on the bridge have degree two and form the sole communication pathway between the two bells. The task requires each node to predict the average input feature of the nodes belonging to the opposite bell. This setup explicitly stresses the model’s ability to transmit information across the narrow bridge separating two densely connected regions.

Category	Methods
Classical GNNs	GCN (Kipf & Welling, 2017), GraphSAGE (Hamilton et al., 2017), GAT (Veličković et al., 2018), GIN (Xu et al., 2019), GCN-II (Chen et al., 2020), ChebNet (Defferrard et al., 2016), SIGN (Frasca et al., 2020)
Differential-Equation-Inspired GNNs	DGC (Wang et al., 2021), GRAND (Chamberlain et al., 2021b), A-DGN (Gravina et al., 2023)
Graph Transformers	G-MLPMixer (He et al., 2023), SPEXPFORMER (Shirzad et al., 2024), SG-Former (Wu et al., 2023b), NodeFormer (Wu et al., 2022), Specformer (Bo et al., 2023), GCN-nsampler (Zeng et al., 2019), GAT-nsampler (Zeng et al., 2019), GT (Shi et al., 2021)

Table 4. Overview of baseline methods used for comparison, grouped by category.

Node-level regression performance is measured using mean squared error (MSE), which serves as an indicator of two well-known failure modes in graph neural networks: oversquashing and oversmoothing. High MSE values can be interpreted diagnostically. An MSE of approximately 1 indicates oversquashing, where the limited capacity of the bridge prevents effective information flow between the two bells, causing nodes to rely primarily on local information. Conversely, an MSE around 30 reflects oversmoothing, where excessive message passing leads to collapsed node representations and nearly identical predictions across the graph, overwhelming local distinctions. Intermediate MSE values (e.g., around 0.5) indicate improved information propagation across the bridge and correspond to better overall task performance.

B.3. Employed Baselines

Table 4 summarizes the GNN baselines used for comparison in our experiments, covering classical architectures, differential-equation-inspired models, graph transformers, rewiring-based approaches, and state-space-model-based methods. To ensure a fair comparison, we adopted the hyperparameter configuration of ChebNet reported in (Hariri et al., 2025).

B.4. Illustrating enhanced explainability

We provide further evidence that the learned potential μ helps revealing the strategy used by the network to solve tasks. We consider a dataset of ring graphs and a task that consists in predicting the correct class (among 10) of a query node. This class is encoded as a dirac in the features of a distant answer node. The query and answer nodes are symmetrically positioned so that there are two long paths of equal lengths connecting them. The features along the first path are all-zero, but the features along the second are i.i.d gaussian noise. Clearly, agglomerating information along that second path results in accumulating noise and therefore poor decision making. As can be seen on Figure 3, μ assigns higher values to vertices on the most efficient path from the answer node to the query node — effectively steering signal propagation along meaningful routes, without altering the original graph topology. Specifically, μ successfully suppresses one of the two paths, concentrating signal flow along a single route. Beyond improving predictive performance, the learned potentials offer transparent, interpretable insights into how the model routes information across complex structures.

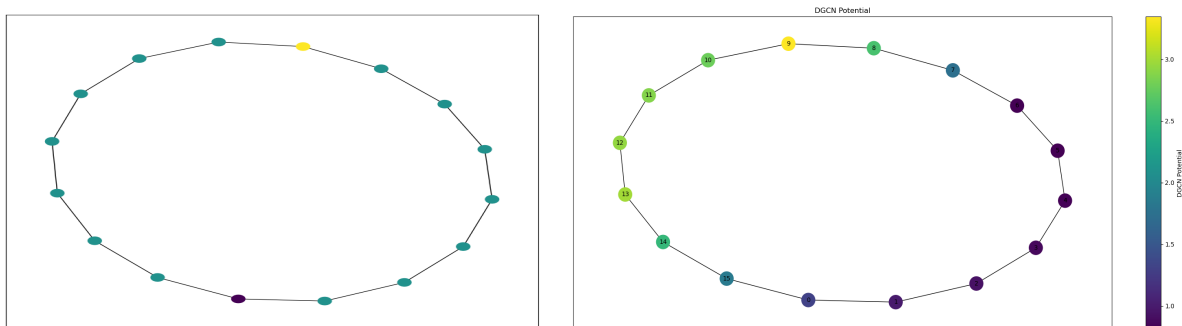


Figure 3. Ring graph configuration. (Left) The query node is in purple and the answer node in yellow. Nodes on the rightward path contain noisy features. (Right) The resulting learned potential has broken the symmetry of the configuration, routing information on the most informative path.